Journal of Materiomics 5 (2019) 663–669

Contents lists available at ScienceDirect

Journal of Materiomics

journal homepage: www.journals.elsevier.com/journal-of-materiomics/

Electrochemical performance of Li_2O-V_2O_5-SiO_2-B_2O_3 glass as cathode material for lithium ion batteries

En-Lai Zhao [a, b], Shi-Xi Zhao [a, *], Xia Wu [a, b], Jing-Wei Li [a, b], Lü-Qiang Yu [a, b], Ce-Wen Nan [b], Guozhong Cao [c, **]

[a] Graduate School at Shenzhen, Tsinghua University, Shenzhen, 518055, China
[b] School of Materials Science and Engineering, Tsinghua University, Beijing, 100084, China
[c] Department of Materials Science and Engineering, University of Washington, Seattle, WA, 98195-2120, United States

ARTICLE INFO

Article history:
Received 26 January 2019
Received in revised form
24 April 2019
Accepted 5 May 2019
Available online 11 May 2019

Keywords:
Lithium ion battery
Cathode materials
Li_2O-V_2O_5-SiO_2-B_2O_3 glass
Electrochemical performance

ABSTRACT

A series of $20Li_2O$-$30V_2O_5$-$(50-x)SiO_2$-xB_2O_3 (mol.%) ($x = 10$, 20, 30, 40) glasses were prepared by the traditional melt-quenching synthesis. The amorphous nature of the glasses was determined by XRD, DSC and TEM investigations. FTIR measurement revealed the functional group of obtained glasses. And EDS results confirmed the presence and uniform distribution of elements in the glasses. $20Li_2O$-$30V_2O_5$-$40SiO_2$-$10B_2O_3$ (LVSB10) sample with the highest V^{4+} ratio exhibited the best cycling capacity. In order to further improve cycling stability of LVSB10 sample, ball milling was employed to reduce the particle size. The ball milled LVSB10 sample (LVSB10-b) showed an improved first discharge capacity, cycling stability and rate capacity. EIS measurements showed that ball milling can effectively decrease charge transfer impedance and facilitate Li^+ ion diffusion. This work provides a new way to explore a new type of cathode materials for lithium ion batteries.

1. Introduction

Lithium ion batteries (LIBs), the important new generation of energy storage devices, have been widely used in portable equipment and electric vehicles due to their high energy density, long cycle life, and low self-discharge rate [1,2]. However, the low capacity and high cost restrict the development of cathode materials [3]. So far, the research on cathode materials are mostly based on crystalline materials, which possess inherent theory capacity, such as $LiNi_{0.5}Mn_{1.5}O_4$ (146.7 $mAh \cdot g^{-1}$) [4], xLi_2MnO_3-$(1-x)LiMO_2$ ($M = Ni$, Co, Mn) (250 $mAh \cdot g^{-1}$) [5], Li_2MnSiO_4 (330 $mAh \cdot g^{-1}$) [6]. It is hard to break the capacity limitations in crystalline materials. Recently, glass materials have been reported as cathode materials due to their capacity controllability by controlling the glass compositions. Furthermore, glass materials have the short-range ordered structure can achieve improved kinetics, the free volume can adapt to large lattice distortion, and the large specific surface area can provide more storage sites, which benefit for electrochemical cycling [7]. In general, oxide glass materials are based on P_2O_5, B_2O_3 and SiO_2 glass formers. P_2O_5-based glasses such as Li_2O-V_2O_5-P_2O_5 [8] and B_2O_3-based glasses such as Li_2O-V_2O_5- B_2O_3 [9] have been investigated as cathode materials. The SiO_2-based glasses are few reported and there is only one research on Li_2O-Fe_2O_3-SiO_2 glass, which shows that SiO_2-based glasses have a stronger network structure compared with B_2O_3-based and P_2O_5-based ones [10]. And vanadium has many accessible oxidation states (V^{5+} to V^{2+}), which can make a high charge/discharge capacity possible [11]. To the best of our knowledge, there are no any investigations on Li_2O-V_2O_5- SiO_2 glass as the cathode material. However, the melting point of SiO_2 is very high ($1650 \pm 50\,^{\circ}C$), which results in a high melting point of the Li_2O-V_2O_5- SiO_2 glass system. Thus, B_2O_3 glass former with a low melting point (450 °C) was employed to reduce the melting point. What's more, borosilicate glasses possess high ionic conduction due to phase separation [12], and B_2O_3 can also decrease the crystallization tendency of the glass materials [13].

In this work, $20Li_2O$-$30V_2O_5$-$(50-x)SiO_2$-xB_2O_3 (mol.%) ($x = 10$, 20, 30, 40) quaternary glass materials were synthesized by a conventional melt-quenching technique. The practicability and limitation of this system glass powders as cathode materials for LIBs were investigated.

* Corresponding author.
** Corresponding author.
E-mail addresses: zhaosx@sz.tsinghua.edu.cn (S.-X. Zhao), gzcao@uw.edu (G. Cao).

Peer review under responsibility of The Chinese Ceramic Society.

https://doi.org/10.1016/j.jmat.2019.05.002

2. Experimental

2.1. Preparation of glass samples

All initial glass samples were prepared by the melt-quenching synthesis. Li_2CO_3 (Analytical grade, Aladdin Chem. Co.), NH_4VO_3 (99%, Macklin Biochem. Co.), SiO_2 (Analytical grade, Macklin Biochem. Co.) and H_3BO_3 (≥99.8%, Aladdin Chem. Co.) were used as lithium, vanadium, silicon, boron sources, respectively. According to the following composition formula: $20Li_2O$-$30V_2O_5$-(50-x)SiO_2-xB_2O_3 (mol%) ($x = 10$, 20, 30, 40), the above raw materials are weighed and mixed. The mixtures were heated at 200 °C for 1 h, ensuring that the raw materials were completely decomposed. The mixtures were melted at 1000 °C for 0.5 h in air. The heating rate was 5 °C/min. Then the melts were quickly poured on a stainless steel plate and pressed by a stainless steel block to obtain thin black glass samples. The samples were hammered, ground and sieved by a 300 mesh sieve to finally get glass powders. Micro vibrating ball mill (MSK-SFM-12M, Kejing Star Tech. Co.) was used to refine particles subsequently under 4000 rpm for 30 min.

2.2. Materials characterization

The structure of the as-prepared glasses were determined by X-ray diffraction (XRD, Rint-2000 V/PC, Rigaku, Japan, Cu Kα radiation: λ = 1.54056 Å) operated at 40 mA and 40 kV, and field emission transmission electron microscope (FE-TEM, Tecnai G^2 F30, FEI 300 kV). Glass transition temperature (T_g) and crystallization temperature (T_c) were measured by differential scanning calorimeter (DSC, NETZSCH STA 449F3 thermal analyzer). The valence states of all the elements were determined by X-ray photoelectron spectra (XPS, Thermo Fisher, ESCALAB 250X), and vibrational bands were confirmed by Fourier transform infrared spectroscopy (FTIR, 3000 Hyperion Microscope with Vertex 80 FTIR System Bruker). And scanning electron microscope (SEM, Carl Zeiss, ZEISS SUORA®55) with an energy dispersive spectrometer (EDS) was used to reveal the morphology and element distribution of the samples.

2.3. Electrochemical characterization

The glass powders were mixed with acetylene black (Super P) and polyvinylidene fluoride (PVDF) in the solvent N-methyl-2-pyrrolidone (NMP), with a mass ratio of 8:1:1, to obtain a slurry. The obtained slurry was coated on aluminum foil, controlling thickness to about 90 μm with a doctor blade. After drying at 120 °C for 11 h in vacuum, the sheet was cut into circular discs with a diameter of 12 mm. 2032 coin-type half cells were assembled in an argon-filled dry box (Universal (2440/750), Mikrouna, China), by using discs above as cathode, lithium foil as counter/reference electrode, Celgard 2300 as separator, 1M solution of $LiPF_6$ dissolved in a mixture of 3: 7 by volume of ethylene carbonate (EC) and dimethyl carbonate (DMC) with 1.0 wt% high voltage additive (Shenzhen CAPCHEM Technology Co. Ltd., China) as electrolyte. All the cells were measured on a LAND CT2001A battery test system at room temperature (25 °C). And a CHI 660D electrochemical workstation was used for electrochemical impedance spectroscopy (EIS) from 100 kHz to 0.01 Hz, at AC voltage of 5 mV.

3. Result and discussion

3.1. Structure and morphology analysis

The XRD results of as-quenched glass powders are shown in Fig. 1. $20Li_2O$-$30V_2O_5$-(50-x)SiO_2-xB_2O_3 ($x = 10$, 20, 30, 40) are named as LVSB10, LVSB20, LVSB30 and LVSB40 sample, respectively. In the XRD patterns, all samples exhibit a characteristic broad hump at about 20° without any Bragg reflections, which indicates that all of the glass powders are amorphous.

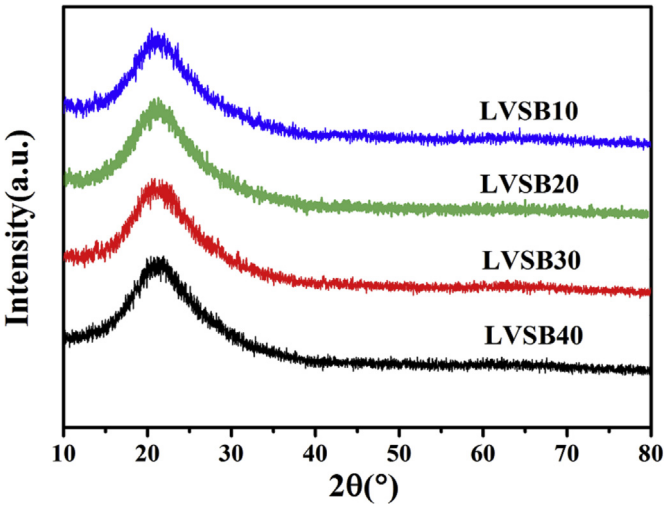

Fig. 1. XRD patterns of LVSB10, LVSB20, LVSB30 and LVSB40 glass samples.

The DSC curves in Fig. 2a reveal the glassy property of the glass samples. The endothermic dips at around 200 °C are attributed to the glass transition, and exothermic peaks at around 230 °C and 310 °C are due to the crystallization. In detail, the glass transition temperature (T_g) is 204 °C for LVSB10, 195 °C for LVSB20, 187 °C for LVSB30 and 181 °C for LVSB40. And the crystallization temperature (T_c) followed T_g is 236 °C, 235 °C, 228 °C and 218 °C, respectively. There is an increase in T_g with the content of Si increases, which should be due to a more stable network structure in SiO_2-based glasses than that in B_2O_3-based glasses as mentioned [10]. Therefore, the more Si content, the stronger glass network structure is, thus the higher T_g is. Furthermore, ΔT ($= T_c$-T_g) of all glass samples are very small, which exhibits a low thermal stability against crystallization [14].

The FTIR spectra of glass samples between 400 and 4000 cm^{-1} are depicted in Fig. 2b. The bands positions in spectra are varied slightly, comparing with criterion values. The band centered at 447 cm^{-1} is associated with the bending vibration of Si-O-Si linkages in [SiO_4] tetrahedron [15]. The band centered at 696 cm^{-1} is assigned to the bending vibration of B-O-B linkages in [BO_3] units [16]. And the band located at 1085 cm^{-1} is ascribed to the asymmetric stretching vibration of Si-O-Si bond in [SiO_4] tetrahedron [17]. The band near 1407 cm^{-1} corresponds to the asymmetric stretch mode of B-O bond in [BO_3] units in different borate groups [18]. The bands at 954 and 761 cm^{-1} are characteristic of presence of V^{5+} in isolated [VO_6] octahedron [19].

The oxidation states of V in glass samples are further studied by XPS investigations. All the XPS spectra are corrected by shifting the C1s peak to 284.8 eV. Fig. S1 is the full scan spectra of glass samples, which shows the existence of Li, V, Si, B and O. Fig. 3 displays the XPS high resolution spectrum of the V $2p_{2/3}$ [20].

As shown, the higher doublets at 517.65 eV should be assigned to V^{5+}, while the lower ones are associated to V^{4+}. Based on the fitting results, the fraction of V^{4+} in all vanadium is 8.68% for LVSB10, 7.13% for LVSB20, 6.45% for LVSB30, and 3.6% for LVSB40, respectively. It is speculated that melting points are different for

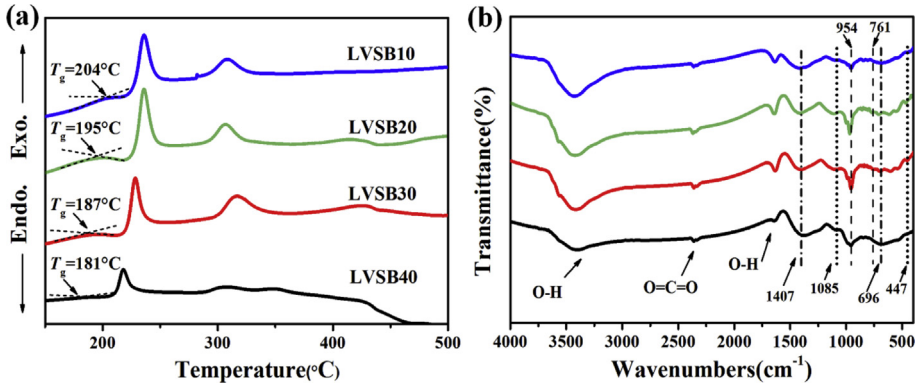

Fig. 2. (a) DSC curves, (b) FTIR spectra of LVSB10, LVSB20, LVSB30 and LVSB40 glass samples.

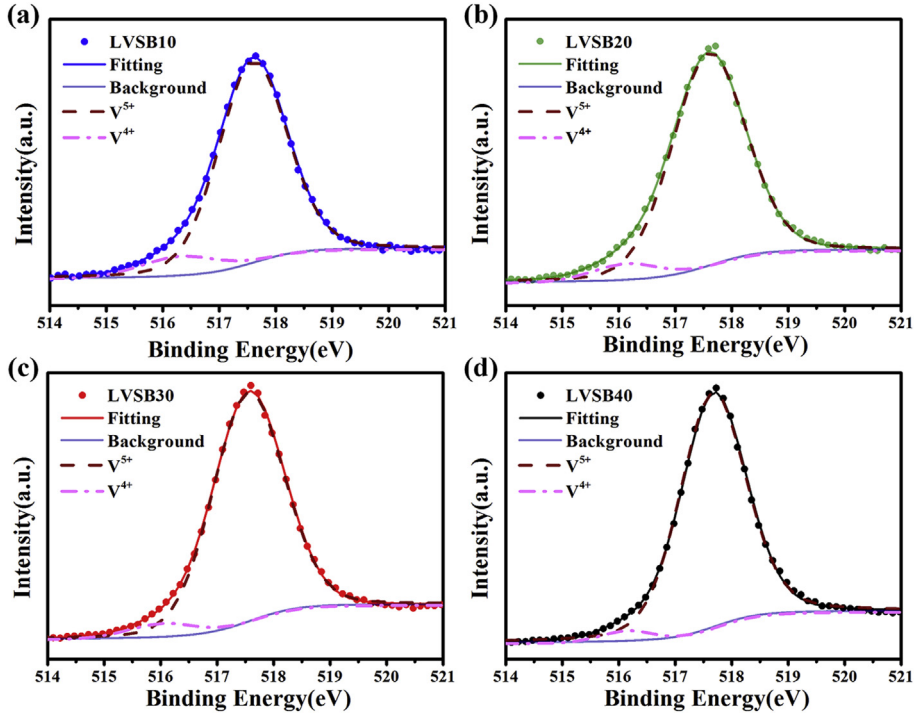

Fig. 3. V $2p_{2/3}$ XPS spectra of (a) LVSB10 glass sample, (b) LVSB20 glass sample, (c) LVSB30 glass sample and (d) LVSB40 glass sample.

different components. Thus, for the same melting temperature, the melting states for different samples are dissimilar, so the ratios of V^{4+} are not same. This phenomenon is also discussed in MoO_3-P_2O_5 glass [21].

Taking LVSB10 sample as an example, the SEM, grain size distribution diagram and HRTEM image are displayed in Fig. 4. It can be seen from Fig. 4(a–b) that LVSB10 sample consists of micron-sized particles with low homogeneity. The result of EDS elemental mappings in Fig. 4c shows that V, Si, B and O elements are uniformly distributed. And the tap density of the LVSB cathode particles was measured by the fully automatic tap density analyzer (Micromeritics, GeoPyc 1360), LVSB10 sample are given as an example (1.3577 g cm^{-3}). In Fig. 4d, no lattice fringes can be observed by high resolution TEM, and there is also no diffraction spot in SEAD patterns, which further confirms the amorphous state of LVSB10. And the same phenomenon can be observed in other samples (Fig. S2).

3.2. Electrochemical analysis

In order to compare the cycling performance of the as-quenched glass cathode materials, Fig. 5(a–b) display the charge/discharge curves at 1st and 50th cycles in the voltage range of 1.5–4.2 V with the current density of 50 mA·g^{-1}. At 1st cycle, all samples show a low charge capacity less than 50 mAh·g^{-1}. The discharge capacity of LVSB10, LVSB20, LVSB30 and LVSB40 samples is 123.7 mAh·g^{-1}, 51.5 mAh·g^{-1}, 37.9 mAh·g^{-1} and 19.5 mAh·g^{-1}, respectively. Fig. S3 gives the cycling performance with gravimetric and volumetric energy densities of LVSB10 sample, the value of which in the first cycle are 360.9 Wh·kg^{-1} and 490.0 Wh·L^{-1} through calculating from the mass and volume of cathode active material. It can be seen that the initial Coulombic efficiency of LVSB glass cathode is unusual. The *ex-situ* XPS spectra of LVSB10 electrode after 1st discharge/charge were shown in Fig. 5c and 5d to explain the unusual phenomenon. After first charge (Fig. 5c), the V $2p_{2/3}$ XPS

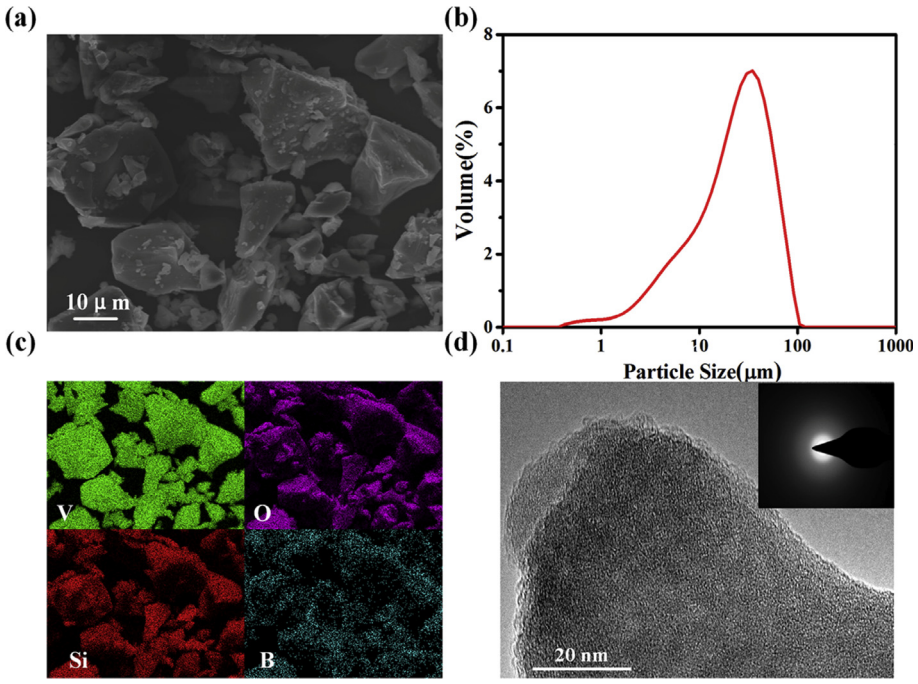

Fig. 4. (a) SEM image, (b) grain size distribution diagram, (c) corresponding EDS result, (d) HRTEM image at high resolution and corresponding SAED pattern (inset) of LVSB10 glass sample.

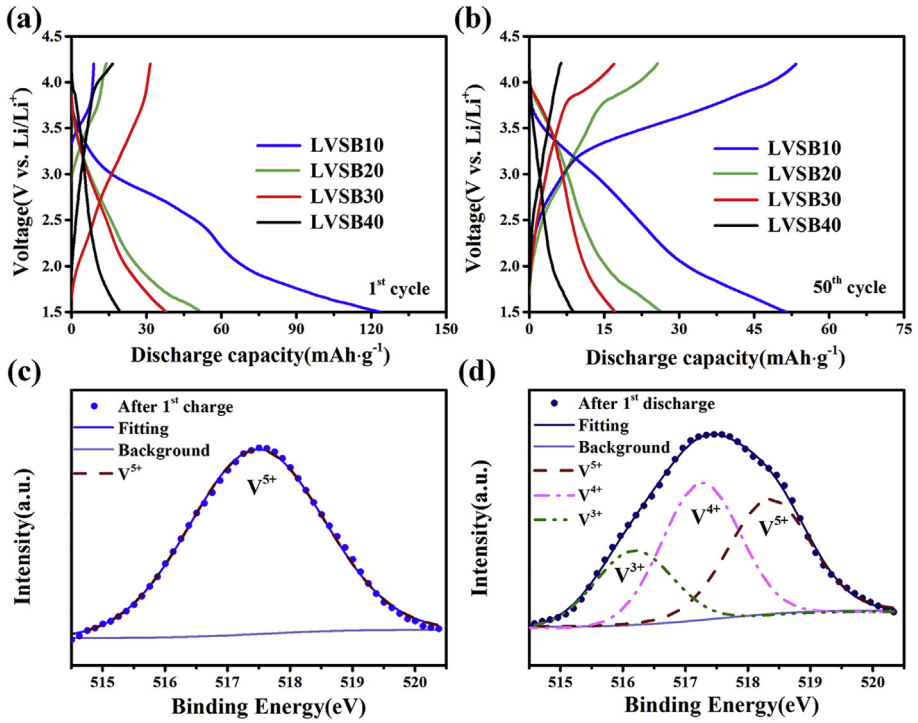

Fig. 5. The charge/discharge curves of LVSB10, LVSB20, LVSB30 and LVSB40 glass samples after (a) 1st cycle, (b) 50th cycle and *Ex-situ* V $2p_{2/3}$ XPS spectra of LVSB10 electrode at (c) 4.2 V and (d)1.5 V for first cycle.

spectrum in LVSB10 electrode is characteristic for V^{5+}. As mentioned in Fig. 3, all the LVSB samples contains a small amount of V^{4+}. When charged up to 4.2 V, only 8.68% V^{4+} in LVSB10 electrode can be oxidized to V^{5+} and thus contribute to a low charge capacity (8.9 $mAh \cdot g^{-1}$). That is, the amount of the electrochemically active V is low during 1st cycle. After first discharge (Fig. 5d), V $2p_{2/3}$ XPS spectrum should be deconvoluted into three spinorbit doublets. The peaks at 518.34 eV, 517.17 eV and 516.14 eV are characteristic for V^{5+}, V^{4+} and V^{3+} [22], and the amount of which is 41.28%, 44.63% and 14.09%, respectively. The

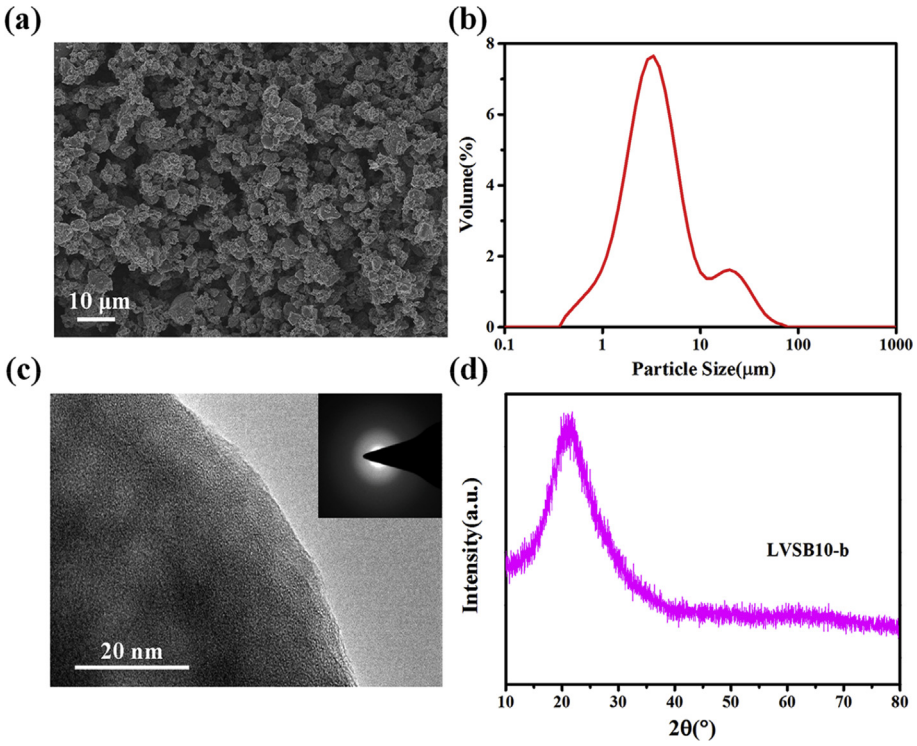

Fig. 6. (a) SEM image, (b) grain size distribution diagram, (c) HRTEM image at high resolution and corresponding SAED pattern (inset), (d) XRD pattern of LVSB10 glass sample.

amount of the electrochemically active V increase, which results in a high discharge capacity (123.7 $mAh \cdot g^{-1}$), and thus presents an unusual initial Coulombic efficiency. However, the Coulombic efficiency gradually become normal, which is 98% for 2nd cycle.

In Fig. 5a, it can also be seen that LVSB10 sample has a much higher initial discharge capacity than other samples. The reason should be ascribed to the higher V^{4+} ratio in LVSB10 sample. In addition, the more V^{4+} generally can present more small polaron hopping, and thus achieve a higher conductivity [23].

However, the glass cathode materials suffer from rapid capacity decay. After 50 cycles, the capacity of LVSB10, LVSB20, LVSB30, and LVSB40 reduce to 51.5 $mAh \cdot g^{-1}$ (248.2 $Wh \cdot kg^{-1}$, 337.0 $Wh \cdot L^{-1}$),

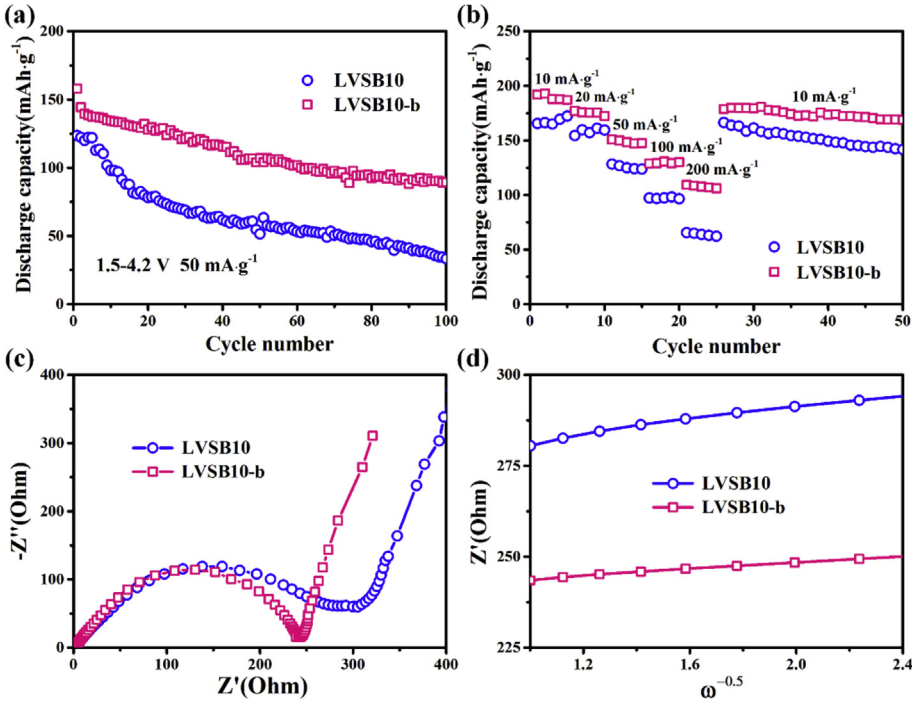

Fig. 7. (a) The cycling performance, (b) rate capacity, (c) Nyquist plots and (d) corresponding Z' - $\omega^{-0.5}$ plots of LVSB10 glass sample and LVSB10-b sample.

26.2 mAh·g^{-1}, 17.4 mAh·g^{-1} and 8.8 mAh·g^{-1}, with a capacity retention rate of 41.6%, 50.9%, 45.9% and 45.1%, respectively, as shown in Fig. 5b. These results demonstrate that the LVSB glass cathode materials have the electrochemical activity with a poor cycling performance, which may be due to the volume change during Li^+ ions insertion and extraction [24], and the low electronic conductivity caused by big particle size [25].

Thus, LVSB10 sample was taken to be ball milled, and the sample obtained was named as LVSB10-b. The reduction in particle size was clearly observed by SEM in Fig. 6a and grain size distribution diagram in Fig. 6b. There are no obvious crystalline peaks and SEAD spots in Fig. 6c, and the XRD results of LVSB10-b sample in Fig. 6d also show that the amorphous properties are maintained after ball milling. The electrochemical performance of both LVSB10 and LVSB10-b samples are exhibited for comparison in Fig. 7.

Fig. 7a shows cycling performance of LVSB10 and LVSB10-b samples in the voltage range of 1.5–4.2 V with the current density of 50 mA·g^{-1}. Obviously, LVSB10-b sample presents an excellent cycling performance, which is better than that of LVSB10 sample. In detail, the specific capacity increases from 123.7 to 158.1 mAh·g^{-1} for first cycle, 98.1 (79.3%) to 134.5 mAh·g^{-1} (85.1%) for 10th cycle, 51.5 (41.6%) to 107.1 mAh·g^{-1} (67.7%) for 50th cycle, and 33.3 (26.9%) to 89.4 (56.5%) for 100th cycle. The rate capability of LVSB10 and LVSB10-b were evaluated at different rates ranging from 10 to 200 mA g^{-1}, and the results are shown in Fig. 7b. At current density of 10, 20, 50, 100 and 200 mA g^{-1}, the specific capacity is about 165, 160, 125, 95 and 65 mAh·g^{-1} for LVSB10 sample, and 190, 175, 150, 130 and 105 mAh·g^{-1} for LVSB10-b sample. After ball milling, LVSB glass cathode materials with refining particles can show better cycling stability and rate capability. It is speculated that the electron and Li^+ ion transport channels are shortened by reducing the particle size, which can effectively improve the conductivity of electrode materials [25]. The enhancement in conductivity corresponds to the improvement of capacity, cycling performance, and rate capability of LVSB glass. In order to confirm the hypothesis in conductivity, Nyquist plots collected by EIS measurement are given in Fig. 7c and corresponding Z' - $\omega^{-0.5}$ plots are displayed in Fig. 7d. There is a depressed semicircle that reflecting charge transfer impedance and an oblique line for Li^+ ions diffusion behavior for each curve [26]. LVSB10-b sample has a smaller semicircle as shown in Fig. 7c, and a less sloped curve as shown in Fig. 7d, which indicates that reduction of particle size in the glass cathode materials by ball milling can decrease charge transfer impedance and enhance Li^+ ions diffusion, thus increase conductivity.

4. Conclusions

A series of $20Li_2O$-$30V_2O_5$-(50-x)SiO_2-xB_2O_3 (mol.%) (x = 10, 20, 30, 40) glasses were prepared by a simple melt-quenching method. XRD, DSC, FTIR, TEM and EDS results revealed the amorphous nature of as-quenched glass powders and uniform distribution of V, Si, B, O elements. And XPS results showed that samples with different Si, B ratios have different V^{4+} fractions. Among the glass materials, $20Li_2O$-$30V_2O_5$-$40SiO_2$-$10B_2O_3$ (LVSB10) sample contained the highest V^{4+} fraction, and thus showed the best electronic conductivity. The initial discharge capacity and cycling capacity of LVSB10 sample were much higher than other samples, however, suffered from rapid capacity decay. Therefore, LVSB10 sample was disposed by ball milling to downsize particles. It was found that the particle size was reduced without changing its amorphous nature. As a result, the discharge capacity of ball milled sample (LVSB10-b) was increased, cycling performance and rate capability were much improved, which is due to decreased charge transfer impedance and the increased Li^+ ion diffusion. In conclusion, Li_2O-V_2O_5-SiO_2-B_2O_3 quaternary glass materials have the potential to become a promising cathode material.

Conflicts of interest

There are no conflicts of interest to declare.

Acknowledgment

This work has been financially supported by Shenzhen Basic Research Project Funds (JCYJ20170817161127616).

Appendix A. Supplementary data

Supplementary data to this article can be found online at https://doi.org/10.1016/j.jmat.2019.05.002.

References

[1] Armand M, Tarascon JM. Building better batteries. Nature 2008;415:652–7.
[2] Goodenough JB, Kyu-Sung P. The Li-ion rechargeable battery: a perspective. J Am Chem Soc 2013;135:1167–76.
[3] Stanley WM. Lithium batteries and cathode materials. Chem Rev 2004;35:4271–301.
[4] Bi K, Zhao SX, Huang C, Nan CW. Improving low-temperature performance of spinel $LiNi_{0.5}Mn_{1.5}O_4$ electrode and $LiNi_{0.5}Mn_{1.5}O_4/Li_4Ti_5O_{12}$ full-cell by coating solid-state electrolyte Li-Al-Ti-P-O. J Power Sources 2018;389:240–8.
[5] Guo ST, Zhao SX, Bi K, Deng YF, Xiong K, Nan CW. Research on electrochemical properties and fade mechanisms of Li-rich cathode materials at low-temperature. Electrochim Acta 2016;222:1733–40.
[6] Wei L, Zhao SX, Wu X, Zhao SJ, Nan CW. The existence form and synergistic effect of P in improving the structural stability and electrochemical performance of $Li_2Mn_{0.5}Fe_{0.5}SiO_4$/C cathode materials. J. Materiomics 2018;4:179–86.
[7] Mathew V, Kim S, Kang J, Gim J, Song J, Baboo JP, Park W, Ahn D, Han J, Lin G. Amorphous iron phosphate:potential host for various charge carrier ions. NPG Asia Mater 2014;6:e138. https://doi.org/10.1038/am.2014.98.
[8] Delaizir G, Seznec V, Rozier P, Surcin C, Salles P, Dollé M. Electrochemical performances of vitreous materials in the system Li_2O-V_2O_5-P_2O_5 as electrode for lithium batteries. Solid State Ionics 2013;237:22–7.
[9] Afyon S, Krumeich F, Mensing C, Borgschulte A, Nesper R. New high capacity cathode materials for rechargeable Li-ion batteries: vanadate-borate glasses. Sci Rep 2014;4:7113.
[10] Togashi T, Honma T, Shinozaki K, Komatsu T. Electrochemical performance as cathode of lithium iron silicate, borate and phosphate glasses with different Fe^{2+} fractions. J Non-Cryst Solids 2016;436:51–7.
[11] Delmas C, Cognac-Auradou H, Cocciantelli JM, Ménétrier M, Doumerc JP. The $Li_xV_2O_5$ system: an overview of the structure modifications induced by the lithium intercalation. Solid State Ionics 1994;69:257–64.
[12] Sun HL, Kang IC, Choi JB, Dong WS. Phase separation and electrical conductivity of lithium borosilicate glasses for potential thin film solid electrolytes. J Power Sources 2006;162:1341–5.
[13] Kim CE, Hwang HC, Yoon MY, Choi BH, Hwang HJ. Fabrication of a high lithium ion conducting lithium borosilicate glass. J Non-Cryst Solids 2011;357:2863–7.
[14] Hassaan MY, Salem SM, Moustafa MG. Study of nanostructure and ionic conductivity of $Li_{1.3}Nb_{0.3}V_{1.7}(PO_4)_3$ glass ceramics used as cathode material for solid batteries. J Non-Cryst Solids 2014;391:6–11.
[15] Daguano JKMB, Milesi MTB, Rodas ACD, Weber AF, Sarkis JES, Hortellani MA, Zanotto ED. In vitro biocompatibility of new bioactive lithia-silica glass-ceramics. Mater Sci Eng: C 2019;94:117–25.
[16] Wang M, Fang L, Li M, Li A, Zhang X, Hu Y, Liu Z, Dongol R. Glass transition and crystallization of ZnO-B_2O_3-SiO_2 glass doped with Y_2O_3. Ceram Int 2019;45:4351–9.
[17] Gao X, Zhang Q, Yu J, Tang W, Li Y, Lu A. Effect of replacement of Al_2O_3 by Y_2O_3 on the structure and properties of alkali-free boro-aluminosilicate glass. J Non-Cryst Solids 2018;481:98–102.
[18] Hao X, Luo Z, Hu X, Song J, Tang Y, Lu A. Effect of replacement of B_2O_3 by ZnO on preparation and properties of transparent cordierite-based glass-ceramics. J Non-Cryst Solids 2016;432:265–70.
[19] Chen Z, Dai C, Gang W, Nelson M, Hu X, Zhang R, Liu J, Xia J. High performance LiV(PO)/C composite cathode material for lithium ion batteries studied in pilot scale test. Electrochim Acta 2010;55:8595–9.
[20] Zhu QY, Chen W, Xu Q, Mai LQ. Novel preparation and XPS analysis of V_2O_5 xerogel. J Wuhan Univ Technol -Materials Sci Ed 2003;18:27–9.
[21] Wu X, Zhao S-X, Yu L-Q, Li J-W, Zhao E-L, Nan C-W. Lithium storage behavior of MoO_3-P_2O_5 glass as cathode material for Li-ion batteries. Electrochim Acta 2019;297:872–8.
[22] Hryha E, Rutqvist E, Nyborg L. Stoichiometric vanadium oxides studied by

XPS. Sur Interface Anal 2012;44:1022–5.
[23] MORI Hidetsugu, MATSUNO Hiroshi, SAKATA Hironobu. Small polaron hopping conduction in V_2O_5-Sb-TeO_2 glasses. J Non-Cryst Solids 2000;276:78–94.
[24] Uchaker E, Zheng YZ, Li S, Candelaria SL, Hu S, Cao G. Better than crystalline: amorphous vanadium oxide for sodium-ion battery. J Mater Chem A 2014;2:18208–14.
[25] Saiful IM, Fisher CAJ. Lithium and sodium battery cathode materials: computational insights into voltage, diffusion and nanostructural properties. Chem Soc Rev 2013;43:185–204.
[26] Wu X, Zhao S-X, Wei L, Deng H, Nan C-W. Improving the structure stability and electrochemical performance of Li_2MnSiO_4/C cathode materials by Ti-doping and porous microstructure. J Alloy Comp 2018;735:1158–66.

Dr.Shi-Xi Zhao is an associate professor at Graduate Shool at Shenzhen, Tsinghua University. He received his Ph.D. (2002) in materials science from Wuhan University of Technology. From 2002 to 2004, Dr. Zhao engaged in postdoctoral research at the Department of Chemistry, Tsinghua University. From August 2004, he has worked at Graduate Shool at Shenzhen, Tsinghua University. His current research is focused mainly on Li-ion battery and supercapacitor materials, and functional ceramics. He has published over sixty academic paper and holds eight Chinese patents.